Two-wavelength approach for control of coagulation depth during laser tissue soldering

Martin Wehner*, Mirko Aden, Nina Toedter, Beate Rosenkranz
Fraunhofer-Institute for Laser Technology, Steinbachstr. 15, 52074 Aachen, Germany

ABSTRACT

In laser tissue soldering (LTS) protein solutions are used for closing of incisions or fixation of wound dressings. During coagulation and thermal denaturation of the protein solutions their morphology changes significantly such that light is strongly scattered. When scattering becomes major component extinction increases and the optical penetration depth shrinks which could lead to unsufficient coagulation and bonding.

For adaption of extinction during coagulation we are investigating a two-wavelength approach. A strongly absorbed laser wavelength (1540 nm) and weakly absorbed wavelength (980 nm) can be applied simultaneously. Simulation of beam propagation is performed in natural and coagulated state of the solder. The model describes a three-layer system consisting of membrane, solder and phantom. The optical properties are determined by spectrometric measurements both in natural and coagulated state. The absorption coefficient μ_a, scattering coefficient μ_s and anisotropy factor γ are determined by numerical analysis from the spectrometric data. Beam propagation is simulated for 980 nm and 1540 nm radiation with ZEMAX® software based on the Monte Carlo method. For both wavelengths the beginning of the process with a clear solder layer, and the final state characterized by a coagulated solder layer are examined.

The optical penetration depth depends mainly on the optical properties of the solder, which change in the course of coagulation process. The coagulation depth can be varied between 1.5 mm to 3.5 mm by changing the proportion of both laser sources. This leads to concepts for minimizing heat input while maintaining a constant coagulation depth.

Keywords: Beam propagation, bovine serum albumin, laser tissue soldering, coagulation, optical properties, soft tissue phantom, wound dressing.

1. INTRODUCTION

Laser soldering is a promising method to replace suturing for wound closure in many applications. An important feature is the immediate sealing of the wounds which has great advantage for many applications. Eye's incisions can be tightly sealed[1] which is important to prevent leakage due to the intraocular pressure. Suturing often does not reach acute pressure-tight sealing resulting in complications of wound healing. Dural reconstruction is another promising application for laser soldering. Suturing can leak after the closure at the areas between the stiches.[2] The dura mater has to be sealed to prevent the leakage of cerebrospinal fluid and the penetration of pathogens into the intracranial area, which has to be kept sterile. Laser soldering could stand immediately a much higher leakage pressure than suturing. Another application for laser soldering is the wound closure of incisions.[3] The tensile strength measured directly after laser soldering can be comparable to the resulting tensile strength from suturing. The closure of large-area wounds, for example burn wounds, with membranes is required to keep the wet environment needed for wound healing. In comparison to suturing laser soldering results in a reduction of scars[4] and avoids subsequent revisions to remove surgical staples. Since no foreign material like surgical suture material is inserted into the wound less inflammation is induced and the wound healing can be improved.[1, 3]

For wound closure or anastomosis of blood vessels typically a few drops of protein solution ("solder") are applied to the tissue, optionally covered by patch to stabilize the ends of the vessels or to seal a wound. Then the site is irradiated by laser radiation and thermally induced coagulation of proteins result in cross-linking and formation of a stiff bond.

*martin.wehner@ilt.fraunhofer.de; phone +49 241 896-202; fax +49 241 896-121; www.ilt.fraunhofer.de

However the exact mechanism of bonding is not clear[5] and the outcome of laser soldering is often inconsistent with respect to the strength of bonds. There are still issues concerning the functional principle of laser tissue soldering and its practical implementation. The process depends on various parameters as laser wavelength, laser power, solder composition, set-point temperature and dwell time, and many tests are required to determine the optimum parameter set for a certain application.[6]

For improved wound healing it is important to minimize the heat input into the tissue but to assure the formation of a stable interface between tissue and solder. Due to morphological changes induced by coagulation the scattering coefficient increases and the optical penetration depth shrinks. We investigate how to control the coagulation depth under the constraint of a maximum surface temperature when the optical penetration depth shrinks. Our model consists of a soft tissue phantom, a thin solder layer of 0.3 mm in thickness, and a silk membrane on top (see

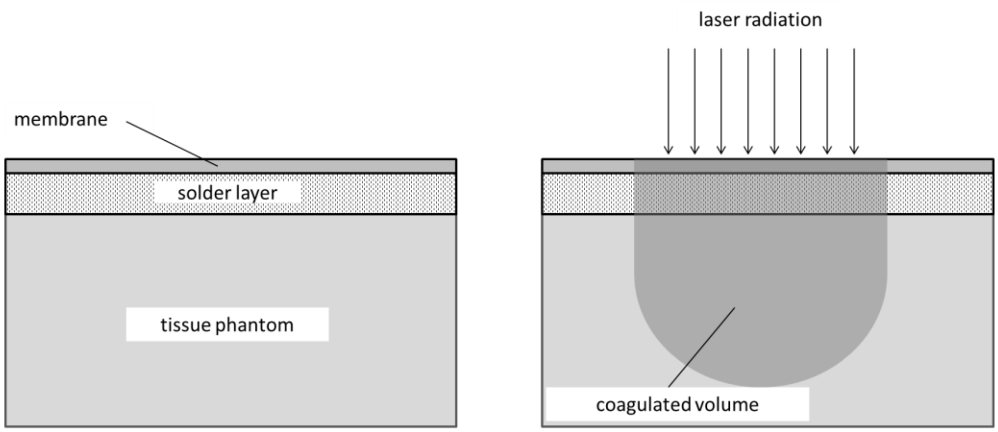

Figure 1).

Before coagulation the tissue or phantom material is in its natural state. The protein solution (solder) is clear and causes virtually no scattering, the phantom is scattering. After heat input by absorption of laser radiation the morphology changes and a coagulated state will be reached which is characterized by similar absorption properties, but strongly increased scattering. Now the solder layer and phantom are coagulated and strongly scattering.

The optical properties of the different layers are derived from spectroscopic measurements. For analyzing the optical penetration depth we calculate the beam propagation in the natural and the coagulated state. The numerical results are compared to experimental results obtained on the phantom.

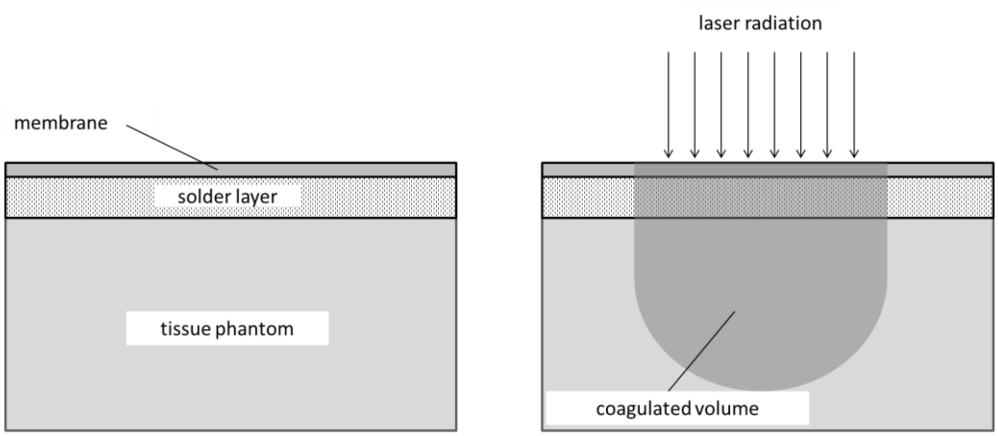

Figure 1: Model of 3-layer system consisting of tissue phantom, solder layer and membrane.

2. MATERIALS AND PREPARATION

2.1 Membrane and solder

Non-woven silk fibroin has been described as a highly human cell-compatible and biodegradable scaffold material which should be a useful for a wide range of target tissues.[7] Artificial silk membranes are produced from silkworm breeding followed by a proprietary bio-casting process developed by Spintec Engineering, Aachen, Germany. The patches are made of bioresorbable ST-Silk membranes in a thickness of 80 µm. The clear membranes show a homogenous structure without any coloration. Before use the membranes are soaked in phosphate buffered saline solution (PBS 41%) for one minute, then put out, allowed to drip off, and laid onto the solder layer on the phantom.

The solder consists of albumin solution which is produced one or two days before use. PBS 41% solution is filled in an Erlenmeyer flask and a small amount of bovine serum albumin (BSA) flakes (Sigma Aldrich, #8076.2) is added. The flask is placed on a magnetic stirrer with a rotational speed of 80 rpm. When the BSA is dissolved the next portions of BSA are added to the solution until a concentration of wt. 42 % BSA is reached. Then the flask is closed and kept in the fridge at 8 °C for one or two days to reduce the foam developed during stirring.

2.2 Phantom

The composition of soft tissue varies from sample to sample due to different concentrations of collagen, melanin, water and blood. Further the thickness of the different tissue layers has an influence on the light propagation.[8] Consequently, there is a large variation of the optical properties determined in other studies, whereas the use of phantoms leads to reproducible results and are storable for up to three months.[9]

For this study the phantom based on the work of Iizuka[10] is chosen which simulates the optical properties of human prostate tissue. It can be fabricated from non-toxic biological materials as chicken egg albumin and bacteriological agar. A major benefit of the phantom is its response to temperatures above 65 °C which is induced by the denaturation of chicken egg albumin. The originally clear structure of the phantom then changes into a strongly scattering material and the volume affected by laser light becomes visible.

For the preparation of the albumin solution the chicken egg albumin (Fluka, #A7641) is dissolved stepwise to 22.2 wt. % in deionized water. Small amounts of albumin are added subsequently to avoid the formation of clots which do hardly resolve. To improve dissolving a magnetic stirrer is used and the rotational speed is set to 80 rpm. After dissolution of the albumin, water is heated up in a second flask to prepare the agar solution. At a temperature of 70 °C 1.4 wt.% agar (amresco, #J637) is added and heated to 85 °C while the magnetic stirring rod is set to a rotational speed of 150 rpm. Afterwards the agar solution was cooled down to 45 °C in a water bath. In the meantime the albumin solution was warmed up to 40 °C. Then the two solutions are mixed and filled into plastic bins to solidify. After two hours the gel got a high viscosity and the phantom became ready for use. Before use the samples were stored in the fridge for a maximum of one week after preparation.

3. OPTICAL PROPERTIES

The optical properties required to simulate beam propagation are absorption coefficient, scattering coefficient, scattering function and refractive index. The absorption and scattering coefficients describe the mean free path of a photon before an absorption or scattering event takes place, the scattering function gives the most probable direction of the scattering event[11] If the radiative transport equation is solved in the four-flux approximation/model, the scattering function reduces to the anisotropy factor γ, which can obtain any value between -1 and 1. For positive values γ describes forward scattering, for negative values backward scattering.[11, 12]

To obtain the optical properties total transmission T, total reflection R and small angle transmission T_d have to be measured. The measurements were performed with a UV-Vis-NIR-spectrometer and an integrating sphere since T and R describe radiation scattered in a large solid angle. From these data absorption coefficient μ_a, scattering coefficient μ_s and anisotropy factor γ are calculated. The details of the experimental setup and the calculations based on the four-flux model are described elsewhere[13] in detail. Measurements and calculations have been made for solder samples in a coagulated state only because solder solutions are virtually not scattering and the absorption coefficient is not expected to change significantly.[10] For the phantom the natural and coagulated states have been investigated since scattering occurs in both states.

For measurement the materials are positioned between two glass slides (Carl Roth GmbH & Co. KG, #H869, index of refraction n_{glass}= 1.53) and mounted on the integrating spheres. The noise signal of the spectrometer setup does not exceed 1% of R or T values. To simplify the calculations the difference in the refraction indices of solder, phantom and glass are neglected because they do not vary much from each other (cp. Table 1). Therefore, the three-layer-system glass/solder (or phantom)/glass can be handled as a single layer with thickness of the solder or phantom, respectively. The surface reflectance of this system is then given by the glass/air interface with n=1.53.

Generally, the absorption coefficient μ_a is smaller for 980 nm than for 1540 nm in both states. In case of solder scattering is negligible for 1540 nm, while for 980 nm the scattering coefficient is larger than the absorption coefficient, but the light-matter interaction is weak for this wavelength. For the phantom scattering becomes more import in the coagulated state. For both materials the anisotropy factor γ is larger than zero, so scattering is forward directed.

Table 1 Optical properties of solder S and phantom P in natural and coagulated state (n,c) for 980 and 1540 nm wavelength; solder layer thickness 1.1 mm, values of refractive indices taken from.[14, 15]

Material	***State***	***D/mm***	***λ/nm***	***T***	***R***	***T_d***	***n***	***μ_a/1/mm***	***μ_s/1/mm***	***γ***
S	c	1,10	980	0,64	0,12	0,40	1,47	0,20	0,56	0,47
S	c	1,10	1540	0,25	0,05	0,21	1,46	1,05	0,30	0,40
P	n	1,10	980	0,75	0,10	0,30	1,44	0,10	0,92	0,69
P	c	1,10	980	0,56	0,24	0,01	1,50	0,10	3,80	0,77
P	n	1,10	1540	0,20	0,05	0,12	1,42	1,10	0,75	0,59
P	c	1,10	1540	0,17	0,06	0,01	1,48	0,80	3,30	0,75

4. SIMULATION OF BEAM PROPAGATION

Once the scattering coefficient μ_s, absorption coefficient μ_a and anisotropy factor γ are known the propagation of radiation in the layered tissue samples can be simulated. For this purpose the ray tracing software ZEMAX®[16] is used where for a large number of rays (>10^6) the propagation of every single ray is monitored. The mean free path of a photon depending on scattering processes is given by the inverse of the scattering coefficient μ_s. The scattering function p is the "Henyey-Greenstein" function depending on the anisotropy factor γ and scattering angle θ[11,17,18]:

$$p(\Theta) = \frac{1}{2}\frac{1-\gamma^2}{\left(1+\gamma^2-2\gamma\cos(\Theta)\right)^{3/2}}, \qquad -\pi < \Theta < \pi.$$

The scattering angle Θ is a random variable which is changed between different events during the simulation. The absorption is handled separately in ZEMAX®. Along a path of propagation the flux of each ray is attenuated exponentially according to the absorption coefficient. Due to the scattering process the length of the optical path varies and can become considerable larger than the geometrical path.

The simulations are carried out for a solder layer of 0.3 mm thickness and a phantom layer of 1.7 mm. The laser beam is rotational-symmetric with top-hat distribution and a diameter of 7 mm. Absorption of laser light results in a production of heat in the layers. ZEMAX® provides a feature to visualize the heat in terms of a power density distribution Q_a.

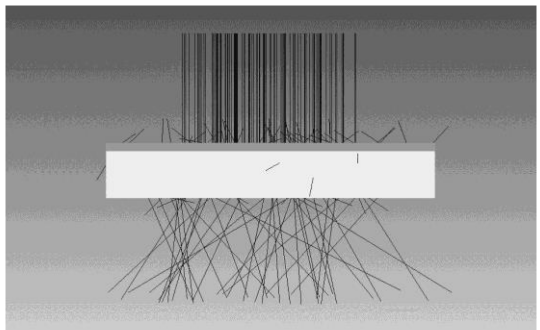

Figure 2 ZEMAX model with trajectories of photons (rotational symmetry); dark grey body: solder (0.3 mm); light grey body: phantom (1.7 mm), diameter of incident beam: 7 mm.

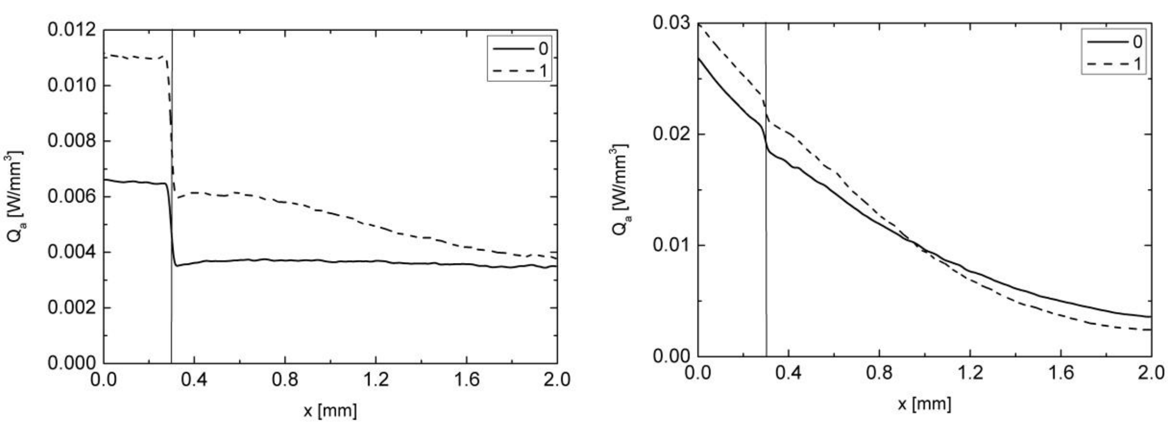

Figure 3: Power density Q_a due to the absorbed laser light along the symmetry axis for 980 nm (left) and 1540 nm (right), 0: natural, 1: coagulated state; position solder: x= 0- 0.3 mm, phantom: x= 0.3- 2 mm, power of incident light 1 W.

In case of 980 nm Q_a is higher in the solder than in the phantom due to the larger absorption coefficient (Table 1). For both materials Q_a is higher in the coagulated state than in the natural state because scattering increases the effective optical path and the probability of absorption. For the solder layer the enhancement of Q_a cannot be explained only by the optical properties of solder. Back scattering from the phantom layer enhances the light flux in the solder layer too. This is indicated by the reflectance R of the coagulated phantom in Table 1. Comparing the values of Q_a at x= 0 and 2 mm indicates that the laser light penetrates deep into the phantom layer for both states. For 1540 nm Q_a is much higher than for 980 nm because the absorption coefficient is larger (Table 1). In the coagulated state scattering in the phantom leads to slightly higher values of Q_a and a slightly smaller penetration depth.

The results can be interpreted in the context of laser soldering in the following way. The power density Q_a drives the heating of the system. In case of a 1540 nm laser heating of solder and phantom will be rapid. (The fate of the membrane is not considered here because the membrane remains stable for temperatures up to 200°C.) To protect the phantom at the solder interface from thermal damage the heat input has to be reduced. This can be done by switching to a laser with 980 nm wavelength. The heat input to the phantom is considerable smaller than for the solder in both states. The lack in interaction can be compensated by enhancing the laser power.

This can be used to control the coagulation depth in phantom tissue. To obtain for example a depth of 1.5 mm 1540 nm radiation will damage the phantom near the solder layer, since Q_a is four times much higher there. Switching to 980 nm will provide a smooth distribution of the power input reaching deeper into the material. The heat generation at the solder/phantom interface is only 1.5 times higher than in 1.5 mm depth.

5. EXPERIMENTAL SET-UP AND RESULTS

5.1 Laser module and controller

The laser set up consists of a fiber-coupled multi-bar laser diode module (type M1F4S22 DILAS GmbH, Mainz, Germany) equipped with (980 +/- 10) nm and (1540 +/- 10) nm diode bars, a controller with two power supplies (type CS408 Amtron GmbH, Wuerselen, Germany) and a homemade handpiece including an infrared temperature sensor (type Optris CT 3M, Optris GmbH, Berlin, Germany), and a lens for collimation of the laser beam.

The handpiece incorporates a Germanium long pass filter $\lambda_c \sim 1650$ nm to reject the laser radiation, whereas the InGaAs sensor covers a spectral range of $2000 < \lambda < 2500$ nm. The radiation from both laser bars is fed into the same optical fiber with a core diameter of 600 µm. The fiber end face is magnified by a f = 30 mm lens to a spot of approximately 7 mm in diameter onto the sample. Two prisms are used to bend the optical axis of the IR sensor beam path and the laser beam path to overlap in the sample area (see Figure 4).

The 980 nm laser bar provides a maximal output power of 50 W and the 1540 nm bar of 12 W. The surface temperature is monitored by the IR sensor and the signal is sent to a digital PID (Proportional-Integral-Derivative) controller which regulates the power of both laser sources (see Figure 3). The measured surface temperature is compared to the set-point temperature and the laser power adjusted accordingly. Typically, a coagulation procedure is performed at a set point temperature of 75 °C to prevent excess heating of tissue. The power ratio of the two laser bars can be fixed at a preset value or altered during the time course.

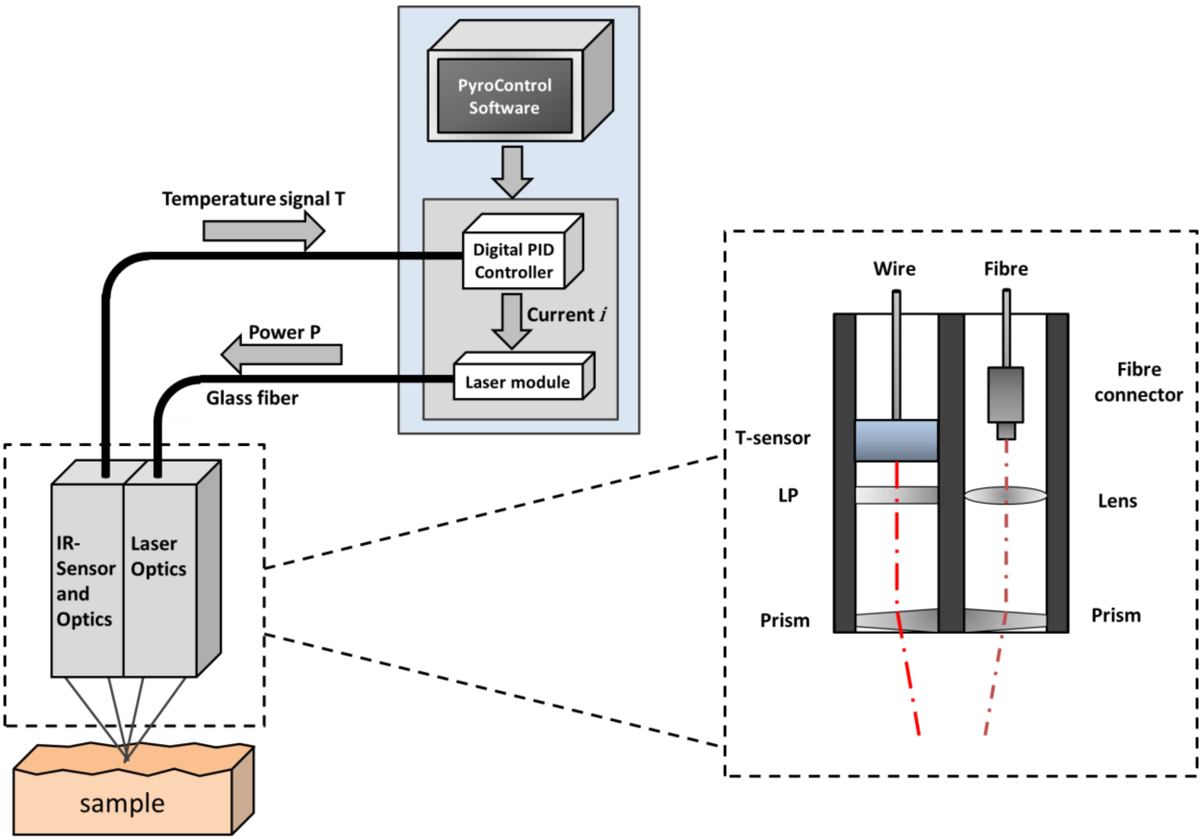

Figure 4: Experimental setup of laser system and handpiece; the surface temperature of the sample is measured by an IR sensor and the laser power regulated by a PID-controller. The GaAs sensor is blocked by a long pass filter LP to reject laser radiation, and two prisms are used to direct the optical paths at the sample.

5.2 Determination of coagulated volume

Irradiation is performed at a setpoint temperature of 75 °C for five seconds. Due to the albumin composition of the phantom the heated volume becomes cross-linked and gets stiff in the coagulated state. The coagulated volume of the phantom is weakly embedded in the non-coagulated part but strongly connected to the membrane by the solder. So the coagulated volume can be taken off easily by pulling the membrane.

The resolved structure is examined by optical microscopy. Figure 5 show samples of the coagulated volume after irradiation with 980 nm and 1540 nm wavelength. The measured height of the coagulated volume is 3.2 mm for 980 nm and 1.5 mm for 1540 nm. The results confirm that the coagulation depth in the phantom tissue can be controlled by the wavelength of the laser radiation for an irradiation time of 5 seconds. The non-planar appearance at 980 nm could be explained by different beam characteristics of the two laser sources. The 1540 nm laser diode bar and coupling optics deliver a broader angular distribution than the 980 nm source. Since the length of the large core fiber is only 3 m, the beam profile is not fully homogenized at the fiber end face.

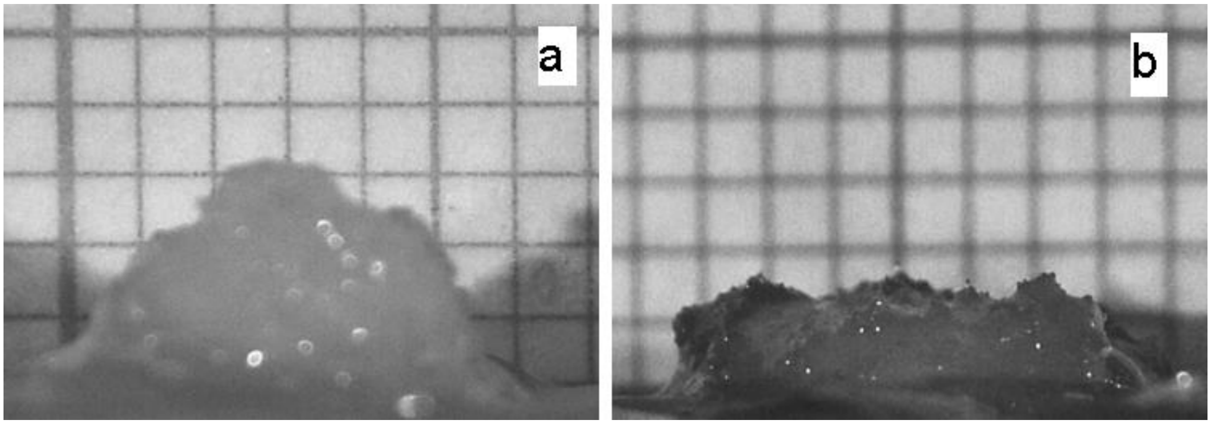

Figure 5: Coagulated volume of the phantom irradiated at 980 nm (a) and at 1540 nm (b); duration 5 s at 75 °C set point temperature; in the background graph paper with 1 mm grid.

6. DISCUSSION AND OUTLOOK

The optical properties of phantom and solder indicate that radiation with a wavelength of 980 nm reach deeper into the tissue than at 1540 nm. This is confirmed by the coagulation experiments of chapter 5. Although a qualitative agreement could be shown, the quantitative relation between the optical penetration depth and the coagulation depth could not be given directly. First of all, heat conduction is not considered in the present investigation. If heat conduction would be considered, the temperatures gradients will be flattened out and deviate from the heat source distribution Q_a shown in Figure 3. Second, the coagulation process itself might change the heat capacity and conductivity of the tissue phantom. A more detailed simulation of laser induced heating and coagulation would require much more information on material properties.

The simple discussion of optical penetration depth can improve the understanding of important features and leads the following procedure for laser wound sealing. The combination of weakly and strongly absorbed laser radiation can be used to mimic laser radiation with intermediate properties. Firstly, the sample surface is heated up fast by the strongly absorbed component of the laser radiation and the set point temperature is reached within about a second. Then a deeper layer is heated up by the weaker absorbed radiation and heat conduction from the hot surface layer. Alternatively, the different laser wavelengths may be applied in sequential order. First, using 1540 nm radiation the solder layer is coagulated within about one second. Then the 1540 nm source is switched off and the 980 nm source is switched on and the laser soldering is performed with additional four seconds. Due to the strong scattering in the solder in the coagulated state the penetration depth of the 980 nm radiation is smaller than at the beginning in the initial state. Further, the power of the 980 nm is reduced because the temperature has already reached the set-point and the temperature control circuit keeps the temperature. Due to the higher penetration depth of the 980 nm radiation the interface between the solder layer and the tissue, respectively phantom, is post cured and strengthened.

LIST OF REFERENCES

[1] Norman, G., Rabi, Y., Assia, E. and Katzir, A., “In vitro conjunctival incision repair by temperature controlled laser soldering,” J. Biomed. Opt. 14(6), 064016 (2009)

[2] Gil, Z., Shaham, A., Vasilyev, T., Brosh, T., Forer, B., Katzir, A. and Fliss, D. M., “Novel laser tissue soldering technique for dural reconstruction,” J. Neurosurg. 103(1), 87-91 (2005)

[3] Brosh, T., Simhon, D., Halpern, M., Ravid, A., Vasilyev, T., Kariv, N., Nevo, Z. and Katzir, A., “Closure of Skin Incisions in Rabbits Laser Soldering II: Tensile Strength,” Lasers Surg. Med. 35(1), 12-17 (2004)

[4] Steinstraesser, L., Wehner, M., Trust, G., Sorkin, M., Bao, D., Hirsch, T., Sudhoff, H., Daigeler, A., Stricker, I., Steinau, H. U. and Jacobsen, F., “Laser-mediated fixation of collagen-based scaffolds to dermal wounds,” Lasers Surg. Med. 42(2), 141-149 (2010)

[5] Simhon, D., Brosh, T., Halpern, M., Ravid, A., Vasilyev, T., Kariv, N., Katzir, A. and Nevo, Z., “Closure of skin incision in rabbits by laser soldering: I: Wound healing pattern,” Lasers Surg. Med. 35(1), 1-11 (2004)

[6] Tabakoglu, H. O. and Gülsoy, M., “In vivo comparison of near infrared lasers for skin welding,” Lasers Med. Sci. 25(3), 411-421 (2010)

[7] Unger, R.E.; Wolf, M.; Peters, K.; Motta, A., Migliaresi, C., Kirkpatrick C. J., “Growth of human cells on a non-woven silk fibroin net: a potential for use in tissue engineering,” Biomaterials 25(6), 1069-1075 (2004)

[8] Anderson, R. R. and Parrish, J. A., “The optics of Human skin,” J. invest. dermatol. 77(1), 13-19 (1981)

[9] Firbank, M., Oda, M. and Deply, D. T., “An improved design for a stable and reproducible phantom material for use in near-infrared spectroscopy and imaging,” Phys. Med. Biol. 40(5), 955-961 (1995)

[10] Iizuka, M. N., Sherar, M. D. and Vitkin, I. A. “Optical Phantom Materials for Near Infrared Laser Photocoagulation Studies,” Lasers Surg. Med. 25(2), 159–169 (1999)

[11] Ishimaru, A., "Wave Propagation and Scattering in Random Media", IEEE/OUP Series on Electromagnetic Wave Theory, Oxford Univ. Press (1997), 0-7803-4717-X

[12] Mudgett, P. S., Richardson, L. W., “Multiple Scattering Calculations for Technology,” Appl. Opt. 10(7), 1485- 1502 (1971)

[13] Aden, M., Roesner, A. and Olowinsky, A., “Optical Characterization of Polycarbonate: Influence of Additives on Optical Properties,” J. Polym. Sci. B Polym. Phys. 48(4), 451-455 (2010)

[14] McNally, K. M., Sorg, B. S., Bhavaraju, N. C., Ducros, M. G., Welch, A. J. and Dawes, J. M., “Optical and thermal characterization of albumin protein solders,” Appl. Opt. 38(31), 6661- 6672 (1999)

[15] Troy, T. L. and Thennadil, S. N., “Optical properties of human skin in the near infrared wavelength range of 1000 to 2200 nm,” J. Biomed. Opt. 6(2), 167–176 (2001)

[16] www.zemax.com (21.05.2012)

[17] Henyey, I. G., Greenstein, J. L., “Diffuse Radiation in the Galaxy,” Astrophys. J. 93, 70- 83 (1941)

[18] Binzoni, T., Leung, T. S., Gandjbakhche, A. H., Rüfenacht, D. and Delpy, D. T., “The use of the Henyey–Greenstein phase function in Monte Carlo simulations in biomedical optics,” Phys. Med. Biol. 51(17), 313–322 (2006)